Clin. Vision Sci. Vol. 6, No. 4, pp. 261–276, 1991
Printed in Great Britain.

0887-6169/91 $3.00 + 0.00

OCULAR DEPENDENCE OF HEMIFIELD VISUAL EVOKED POTENTIALS: RELEVANCE TO BILATERAL CORTICAL REPRESENTATION OF CENTRAL VISION

JONATHAN D. VICTOR,[1,2] MARY M. CONTE[1,2] and COSTANTINO IADECOLA[1]

[1]Department of Neurology and Neuroscience, Cornell University Medical College, 1300 York Avenue and [2]Laboratory of Biophysics, The Rockefeller University, 1230 York Avenue, New York City, NY 10021, U.S.A.

(Received 5 April 1990; in revised form 10 December 1990)

Summary—1. In primates there are cells in the nasal half of the fovea which project to the ipsilateral LGN, and from there presumably to the ipsilateral primary visual cortex (Leventhal *et al.*, 1988; *Science*, **240,** 66–67). Accordingly, the pattern of cortical activation produced by monocular viewing of a single hemifield should depend on the eye which is stimulated.

2. We studied visual evoked potentials (VEPs) elicited by monocular hemifield stimulation in man to determine whether such interocular differences could be detected. Such a difference was indeed present, and (according to a resampling technique) was unlikely to be due to chance alone in 5 of 6 subjects. Dipole modeling showed that this difference was consistent with the pattern of retino-calcarine projections described in primates.

3. We conclude that the bilateral cortical representation of the nasal half of foveal retina found in primates is likely to be present also in man. These results are discussed in relation to binocular vision near the vertical meridian.

Key words—Human; dipole modeling; hemifield; macular sparing; retinocortical projection; visual evoked potentials.

INTRODUCTION

In primates, including man, the ganglion cells of the temporal retina project to the ipsilateral lateral geniculate nucleus (LGN) and primary visual cortex (area 17) while those of the nasal retina project to these structures in the contralateral hemisphere through the optic chiasm (Polyak, 1934; Stone *et al.*, 1973; Bunt *et al.*, 1977). By this arrangement, each cerebral hemisphere receives information from the contralateral visual hemifield. Thus, lesions of the post-chiasmatic visual pathways produce the well-established pattern of loss of vision contralateral to the lesion (Williams and Gassel, 1962).

The segregation pattern of retinal afferents has important consequences for vision at or near the vertical meridian (Hubel and Wiesel, 1967; Blakemore, 1969). If the projections of nasal and temporal retinas remain strictly segregated, there would be a discontinuity in vision at the vertical meridian. Furthermore, areas of space in front of or behind the fixation point would be devoid of binocular vision (Blakemore, 1969). If binocular vision near the vertical meridian is similar to binocular vision off the meridian, the visual information arising from the retina near the meridian must be transmitted to both hemispheres.

There are two mechanisms for the transmission of information near the vertical meridian to both hemispheres: the well-established transcallosal associative projections linking the visual cortices (Hubel and Wiesel, 1967; Wong-Riley, 1974), and bilateral projection of ganglion cells near the retinal midline. The second possibility was proposed many years ago (Morax, 1919), and has recently been supported by retrograde transport studies in monkey (Bunt *et al.*, 1977; Leventhal *et al.*, 1988). Leventhal *et al.* (1988) demonstrated a 0.5 deg wide band of nasal retina near the fovea which contains ganglion cells that project to the ipsilateral LGN, and, presumably, to the ipsilateral striate cortex. Since these cells are intermingled with cells that project contralaterally, this region of the nasal fovea is represented in both hemispheres. Leventhal *et al.* (1988) propose that the double representation of nasal retina

near the fovea may account for the clinical phenomenon of "macular sparing"—preservation of central vision in an otherwise blind hemifield.

This arrangement of retino-geniculate projections predicts that the pattern of cortical activation produced by monocular viewing of one hemifield depends on which eye is stimulated (Fig. 1). Consider viewing of the left hemifield by the right eye. The temporal retina is stimulated, and it projects only to its ipsilateral hemisphere (the right hemisphere). Now consider viewing of the same hemifield by the left eye. The nasal retina is stimulated. The entire nasal retina projects to the contralateral (right) hemisphere. If the primate anatomy near the midline pertains to man, then there is an additional projection of cells from nasal retina near the fovea to the *ipsilateral* (left) hemisphere. In sum, monocular viewing with the eye contralateral to the hemifield activates only the cortex contralateral to that hemifield. But monocular viewing with the eye ipsilateral to the hemifield is predicted to activate a portion of the ipsilateral cortex as well.

In this study, we asked whether this pattern of projections is present in man, and whether it can be detected physiologically. We examined human visual evoked potentials (VEPs) elicited by monocular viewing of fine pattern stimuli restricted to hemifields. Principal component analysis indeed demonstrated a dependence of the VEP topography on the stimulated eye. Dipole modeling revealed that such eye dependence was consistent with the model of retino-geniculate projections described above. Thus, the bilateral foveal representation observed in anatomical studies of primates is likely to be present also in man. We discuss this finding in relation to the clinical controversy of macular splitting and macular sparing, and binocular vision near the vertical meridian.

METHODS

Studies were conducted on 6 normal volunteers (3 males and 3 females) with no history of neurological or neuro-ophthalmological diseases. The age of the subjects ranged from 28 to 40 yr. Three of them were naive to the purpose of the experiments. Visual acuity was corrected to normal if necessary.

Visual stimulation apparatus

The visual stimuli were produced on a Tektronix 608 monitor, whose raster display subtended an 8.8 deg square at a viewing distance of 57 cm. Control signals for the monitor [horizontal (X), vertical (Y) and intensity (Z)] were generated by specialized electronics (Milkman *et al.*, 1980) interfaced to a Digital Equipment Corporation 11/73 computer. This apparatus provided for a 256×256-pixel raster display with a refresh rate of 270.329 Hz.

Each stimulus was a contrast reversing checkerboard restricted to either the left or right hemifield. Checks were 4 min on each side and had a contrast $[(I_{max} - I_{min})/(I_{max} + I_{min})]$ of 0.4. This small check size was used to minimize scatter of modulated light into the unstimulated hemifield. The contralateral hemifield was unmodulated and maintained at the mean luminance of the checkerboard display (150 cd/m^2). An unmodulated dark (< 1 cd/m^2) fixation point 4 min across was incorporated into the precise center of the display screen, extending 2 min into the patterned region and 2 min into the unpatterned region.

Recording of VEPs

Scalp signals were recorded differentially from a line of nine gold cup electrodes applied to the scalp with electrode paste and placed 2.5 cm apart along a horizontal line centered at O_Z (Fig. 2 inset). We designated off-midline electrode locations by L_N or R_N for an electrode N mm to the left or to the right of the midline, respectively. With this notation, our montage was: L_{100}–L_{75}, L_{75}–L_{50}, L_{50}–L_{25}, L_{25}–O_Z, O_Z–R_{25}, R_{25}–R_{50}, R_{50}–R_{75} and R_{75}–R_{100}. These eight signals (derivations) were amplified 10,000-fold and bandpass-filtered (0.1–100 Hz) prior to digitization. Artifact rejection was performed by the computer prior to averaging. VEPs were saved on disk for off-line analysis (see below).

This bipolar montage was chosen in preference to a referential one in order to optimize detection of *differences* in scalp topography across experimental conditions, rather than to maximize the signal-to-noise ratio. In contrast, a referential montage (e.g. all leads referenced to C_z) would likely have provided a larger signal, but poorer resolution of near-field components.

VEPs were elicited by square-wave contrast-reversal of the patterned field at a fundamental frequency of 4.22 Hz (reversal rate of 8.45 Hz). The stimulus duration was 35 s, with averaging

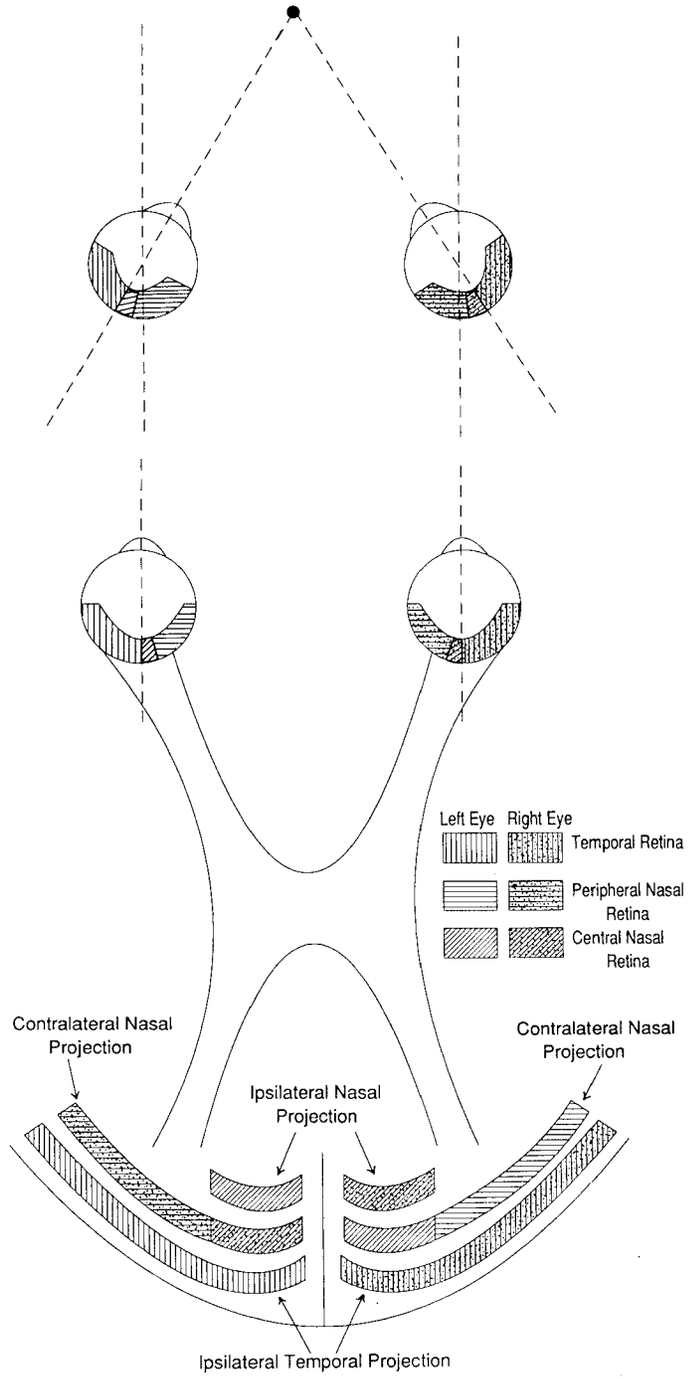

Fig. 1. Lower panel: schematic representation of the primate visual pathways illustrating the pattern of retinocortical projections. Temporal retina projects to the ipsilateral hemisphere. Peripheral nasal retina projects to the contralateral hemisphere. Central nasal retina projects to both contralateral and ipsilateral hemispheres. Viewing of a hemifield through the contralateral eye activates only the hemisphere contralateral to the stimulus. However, viewing of a hemifield through the ipsilateral eye also activates a portion of ipsilateral cortex. Upper panel: when the eyes are converged, the central portion of nasal retina is required to view a wedge of the contralateral hemifield which is behind the fixation point.

of the scalp signals initiated 5 s into the stimulus. Stimuli were presented in the following order: (1) left eye, left hemifield; (2) left eye, right hemifield; (3) right eye, left hemifield; (4) right eye, right hemifield. This sequence was repeated a total of 10 times for each subject. This particular order of stimulation ensures that ocular effects are not confounded with adap-

tation effects: each eye first views the left hemifield and then the right hemifield. The eye that was not viewing the stimulus was covered by a gauze diffusing pad.

RESULTS

Hemifield VEPs

Figure 2 shows the averaged VEPs recorded from one subject. For each hemifield and each eye, steady-state responses were measured at each of the 8 derivations. Responses were typically small (0.3–1.0 μV). Stimulation of a particular hemifield produces larger responses over the contralateral hemisphere. This pattern, rather than the well-known "paradoxical" lateralization of responses to the ipsilateral hemisphere with referential recording (Halliday and Michael, 1970), has previously been reported with bipolar recording (Cobb and Morton, 1970; Barrett *et al.*, 1976). In our recording conditions, the largest signals typically were found in the two paramedian derivations (O_Z–R_{25} and R_{25}–R_{50} for left-field stimulation; L_{50}–L_{25} and L_{25}–O_Z for right-field stimulation).

Since the stimulus was a contrast-reversal pattern, responses were anticipated at even harmonics of the stimulus frequency, with the largest component at the second harmonic of the stimulus frequency. Each waveform shown is the response to one full stimulus cycle (two contrast-reversals), averaged over ten 30-s presentations of each stimulus condition. The correspondence between the first and second halves of the waveform provides a qualitative indication of the signal-to-noise ratio.

To quantify the signal-to-noise ratio, we focused on the second harmonic component. Fourier components, represented as complex numbers, may be considered as vectors in the complex plane. Estimates of the Fourier component from individual runs may be denoted $\mathbf{z}_k$. The Fourier component obtained by averaging across all repeats of a particular condition, denoted $\mathbf{z}$, is the arithmetic mean of the $\mathbf{z}_k$. The variance of the N individual estimates $\mathbf{z}_k$ about their mean $\mathbf{z}$ may be expressed as

$$V_{\text{indiv}} = \frac{1}{N-1} \sum |\mathbf{z}_k - \mathbf{z}|^2.$$

This quantifies the run-to-run variability of individual Fourier estimates. A second variance may be calculated from the group-average Fourier component, $V_{\text{group}} = |\mathbf{z}|^2$. The ratio $S = V_{\text{indiv}}/V_{\text{group}}$ of these two quantities is a quantification of the ratio of signal power to noise power. Under the null hypothesis that no signal were present, it may be shown that the quotient $V_{\text{group}}/V_{\text{indiv}}$ is distributed like $F_{[2,2N-2]}$ (Victor and Mast, 1991). Thus, for a 95% confidence of detection, the critical signal-to-noise ratio is 3.55, and for 99% confidence, the critical signal-to-noise ratio is 6.01. For the data shown in Fig. 2, signal-to-noise ratios ranged from <1 to >40, with a geometric mean (across all derivations and stimulus conditions) of 3.66. Note that the signal-to-noise ratio S, which is a quotient of variances, is essentially a power ratio; the corresponding ratio of signal amplitude to noise amplitude is $\sqrt{S}$, with critical values of 1.88 (95%) and 2.45 (99%) for averages derived from 10 repeats.

The signal-to-noise ratios for the other subjects are summarized in Table 1 by taking the geometric mean of 32 individual signal-to-noise ratios (eight derivations and four stimulus conditions). In all subjects but MW, most responses were clearly resolvable above noise. For MW, the mean signal-to-noise was below the 95% confidence limit, although individual signal-to-noise ratios exceeded the 95% critical value in 10 of the 32 cases. For JV, the mean signal-to-noise was approximately at the 95% confidence limit, and individual signal-to-noise ratios exceeded the 95% critical value in 19 of the 32 cases. For MC, the subject with the highest mean signal-to-noise ratio, individual signal-to-noise ratios exceeded the 95% critical value in 30 of the 32 cases.

Analysis of VEP topography

The next part of the analysis is to compare responses elicited by left-eye and right-eye viewing of each hemifield. A simple approach is to make individual comparisons of Fourier components recorded at each derivation. For example, in the right hemifield responses of subject JV (lower portion of Fig. 2), there is a clear response at L_{25}–O_Z (second harmonic amplitude of 0.25 μV, $S = 12.06$, $P < 0.01$) with left eye stimulation, but no detectable second harmonic response with right eye stimulation (amplitude 0.07 μV, $S = 1.20$, not significant). While this comparison suggests that interocular differences exist, it has several failings. (i) This comparison is *a posteriori*, and fails to account for the number of possible comparisons and possible covariances in estimates of Fourier components across electrodes. (ii) This comparison confounds differences in the overall ampli-

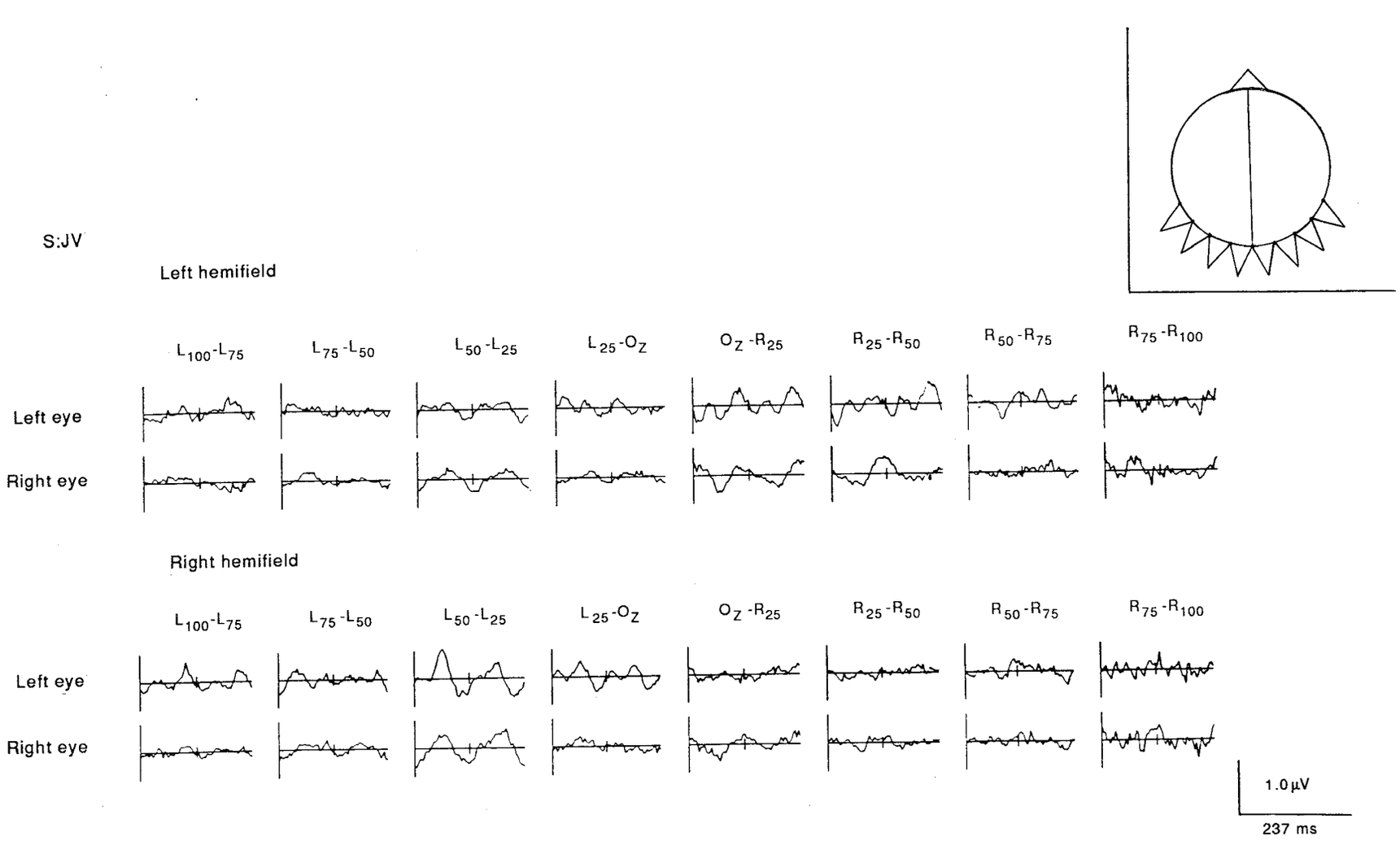

Fig. 2. Bipolar recording of VEPs produced by hemifield stimulation with 4 min contrast-reversing checks. Maximal responses were seen near the midline over the hemisphere contralateral to the stimulated field. Inset: the recording montage used.

Table 1. Overall signal-to-noise ratios, correlation coefficients (r) and estimates of significance levels (P) for scalp distributions of first principal components of monocular hemifield responses in 6 subjects. For each subject, the signal-to-noise ratios listed are geometric means of $S = V_{\text{indiv}}/V_{\text{group}}$, calculated at each of the eight derivations, under each of four experimental conditions. The correlation coefficient r indicates the similarity between the scalp distributions obtained with left and right eye stimulation. Significance levels were derived by a resampling procedure (Efron, 1980) described in the text, in which the correlation coefficients of 1000 resampled scalp distributions were compared with the value of r obtained from the data. Small values of P indicate that most of the resampled values were greater than the measured value of r, which implies that the difference between the distributions obtained from each eye is unlikely to be due to chance alone. An entry of <0.001 for the estimated significance level (P) indicates that none of 1000 resampled hemifield responses led to a smaller value of r

		Left hemifield		Right hemifield	
Subject	Mean S	r	P	r	P
JV	3.66	0.963	0.764	0.496	<0.001
MC	23.79	0.968	<0.001	0.994	0.225
RB	6.64	0.826	0.065	0.988	0.416
KP	21.45	0.971	0.165	0.955	0.001
MW	1.27	0.727	0.196	0.953	0.348
MS	10.69	0.980	0.058	0.974	0.054

tude or dynamics of each eye's response with differences in topography. (iii) This comparison does not make use of higher even harmonics in the response. Therefore, we took a more rigorous, though necessarily more elaborate, approach.

The first step was to calculate the Fourier components at the first four even harmonics of the stimulus frequency ($2f$, $4f$, $6f$ and $8f$) at each electrode. The reason for ignoring odd-order and higher-order even harmonics was to enhance the signal-to-noise ratio. Odd-order Fourier components reflect differences between the first and second halves of each averaged response. Because the stimulus is contrast-reversing, these components contain only noise. Furthermore, under these stimulation conditions, there is little response at $10f$ and even higher harmonics of the input frequencies (Gutowitz *et al.*, 1986, Fig. 1).

The second step was to determine the spatial topography of these waveforms, as reconstituted from their first four even Fourier components. We assumed that the waveforms recorded at each derivation reflect the summed contributions of a small number of mechanisms, with weightings of each mechanism determined by volume conduction. This situation can be analyzed by principal component analysis in the frequency domain (Gutowitz *et al.*, 1986). If only one neural mechanism is present, then the 8 measured waveforms will all be scalar multiples of a common waveform. In this case, the first principal component is defined by the best-fitting common temporal waveform, and a vector of weights $\mathbf{w} = (w_1, w_2, \ldots, w_8)$. The component w_j indicates how the best-fitting temporal waveform should be scaled to provide a fit for the response recorded at the jth derivation. The weights were normalized by $\Sigma w_j^2 = 1$. Subsequent principal components express the deviation of the measured waveforms from these scalar multiples of a common waveform. Such deviations might reflect either systematic deviations or variations due to "noise".

In our data, the first principal component generally contained 70% or more of the response power, and less than 25% of the response power was contained in the second principal component. As judged from the significance levels of the responses themselves (Table 1), the second principal component would therefore be only marginally resolvable above noise. Furthermore, second principal components did not appear to show a consistent pattern either across subjects or within subjects, as assayed by analysis of fractions of the data set. For these reasons, second (and subsequent) principal components will not be analyzed further. By restricting analysis to the first principal component, we do not mean to imply that there is only one source (see Discussion). Rather, restriction of attention to the first principal component provides a summary of scalp topography which respects the noise present in the experimental data.

For each subject and each recording condition, the value of w_j reflects the relative contribution of a best-fitting waveform (specific to that subject and recording condition) to the jth bipolar derivation. Dynamical information is contained only in the shape of the common waveform itself. We ignore this in our analysis, and concentrate on the spatial weights w_j. A zero-crossing of the value of the weight implies that the waveform has undergone polarity inversion. This corresponds to a half-cycle phase shift of all Fourier components in the response, as would be expected in waveforms driven by opposite ends of a dipole.

Spatial weights extracted from the data of Fig. 2 are shown in Part A of Fig. 3. Let us first compare left hemifield responses with right hemifield responses. For left hemifield responses, the largest magnitude weight is in the

two derivations just to the right of the midline (O_Z–R_{25} and R_{25}–R_{50}). For right hemifield responses, the largest weight is in the derivation two positions left of the midline (L_{50}–L_{25}). As previously noted, the contralateral extremum is expected in bipolar recording (Barrett *et al.*, 1976). However, the weights derived from left hemifield and right hemifield stimulation are approximately, but not precisely, mirror-images.

Now let us examine the data more closely, focusing on differences between the weights obtained with each eye. For right hemifield stimulation of the left eye, there is a large (negative) weight present at the derivation just to the left of the midline (L_{25}–O_Z). However, with right eye stimulation, the weight for this derivation is near zero. The difference in the response with left and right eye stimulation is also evident in the waveforms of Fig. 2 (compare fourth tracing in the two bottom rows). No similarly-striking differences are present with left hemifield stimulation.

Before turning to statistical tests of the significance of the eye dependence of response topography, we consider qualitatively the data sets of the other subjects (Fig. 3B and C). For the subject of Panel B, there is virtually no interocular difference in responses to right hemifield stimulation. There is a small difference in response to left hemifield stimulation, at the derivation just to the right of the midline (O_Z–R_{25}). Although this difference is small, it is three times the difference between the weights measured with right hemifield stimulation. As in Panel A, with stimulation of the eye ipsilateral to the field, there is a smaller response at the contralateral paramedian derivation. Both subjects display a larger interocular difference in one hemifield than with the other, as well as asymmetries of left-field and right-field responses within one eye.

Data in Panel C show much the same pattern. There is virtually no interocular difference in weights measured with right hemifield stimulation. There is an interocular difference with left hemifield stimulation, most prominent at the derivation just to the right of the midline (O_Z–R_{25}). Two of the three remaining subjects, KP and MS, had response patterns similar to those of Fig. 3A–C. For the sixth subject (MW), there was no similar indication of an interocular

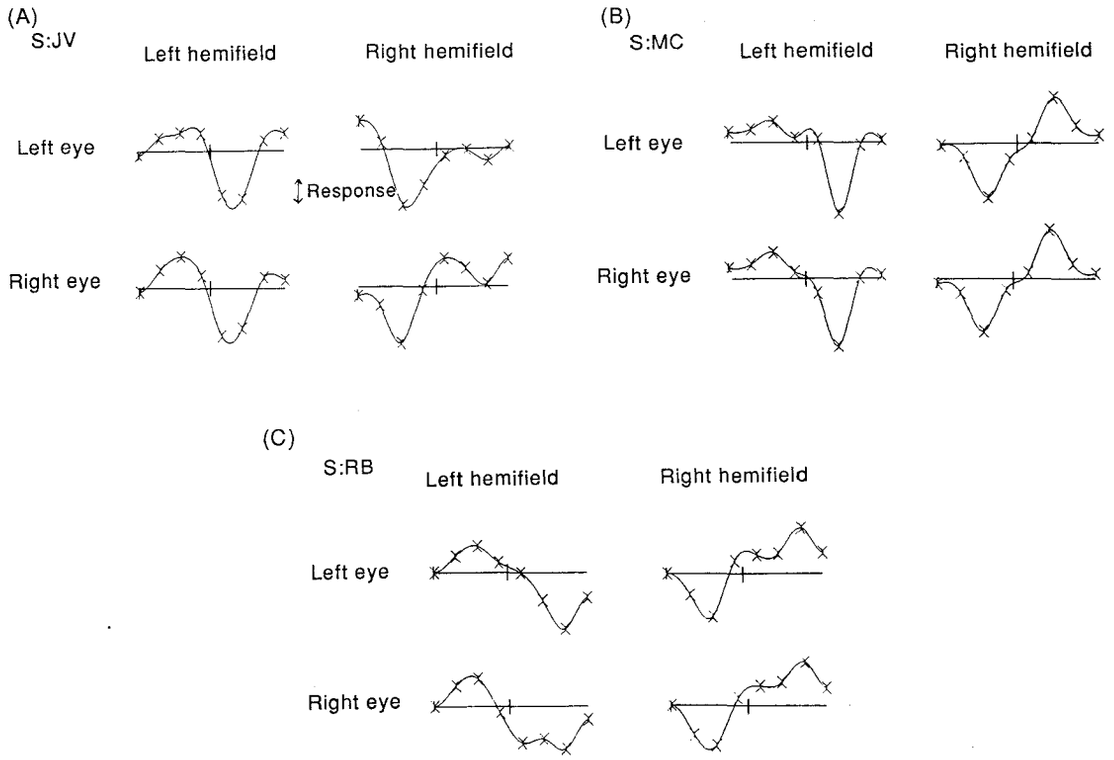

Fig. 3. Scalp topography of monocular hemifield responses. The Xs indicate the eight measured weights for the first principal component, with the left-most X corresponding to L_{100}–L_{75} and the right-most X corresponding to R_{75}–R_{100}. The smooth line is interpolated through these points by a spline (Ahlberg *et al.*, 1967). Weights are normalized to unity power. Data of Part A are calculated from Fig. 2.

difference in weights. This was the subject with the smallest signal-to-noise ratio.

Analysis of interocular differences

To quantify the interocular difference in scalp topography, we calculated the dot-product r between the weights $\mathbf{w}$ recorded with stimulation of the left eye and the weights $\mathbf{w}'$ recorded with stimulation of the right eye. This quantity may be written $r = |\Sigma\, \mathbf{w}_j \cdot \mathbf{w}'_j|$. It is indeed a correlation coefficient, because the weight vectors $\mathbf{w}$ and $\mathbf{w}'$ are normalized. In general, r may be thought of as the cosine of the angle between the two weight vectors $\mathbf{w}$ and $\mathbf{w}'$. The quantity r is also the length of the projection of $\mathbf{w}$ onto $\mathbf{w}'$ or vice versa. For responses with identical topographies, $r = 1$. For responses with different topographies, $r < 1$. Comparisons based on r ignore overall changes in the size of the response, and also ignore interocular differences in temporal waveform.

Values of r for all 6 subjects are shown in Table 1. Other than a single value of $r = 0.496$, the values of r lie in the range 0.727–0.988.

We now assess whether the interocular differences are statistically significant, as measured by the departure of r from 1. This is a departure from the typical kind of significance testing of correlation coefficients, in which the chief question is whether r is significantly different from 0. Because hemifield responses obtained with either eye are similar, r is close to 1. The question of interest is not whether left-eye and right-eye hemifield responses are correlated, but whether the small differences between left-eye and right-eye responses (i.e. the departure of r from 1) are more than would be expected from the variability in the responses themselves.

Although values of r are calculated from Fourier components of the responses themselves, it is difficult to obtain accurate confidence limits on r from the signal-to-noise ratios of the individual Fourier components. Such a calculation would require knowledge not only of the variances of individual Fourier components, but also of covariances of distinct Fourier components (e.g. second-harmonic and fourth-harmonic) within and across derivations. Furthermore, r is related in a complex nonlinear fashion to the measured Fourier components, so that even with exact knowledge of covariances, estimation of confidence limits on r would be difficult.

Therefore, to estimate whether r is significantly different from 1, we used a resampling technique (Efron, 1980) in which the internal variability in the data serves as a means to assess reliability of r. Consider the null hypothesis that the monocular hemifield responses driven by either eye have the same scalp topography. Under this hypothesis, there is a reasonable likelihood that correlation coefficients as small as, or smaller than, the observed value of r would be obtained if the hemifield responses were shuffled randomly between eyes.

We estimated this probability (P) empirically from the data. For each subject, the 20 responses from each hemifield were randomly shuffled and assigned arbitrarily to the "left eye" or the "right eye" of a "resampled" data set. In the resampling process, responses at different electrode derivations were *not* scrambled; rather, entire 30-s runs were randomly re-labeled as to which eye was stimulated. Thus, if scalp topography were independent of eye of stimulation, then the interocular difference observed in the actual data set should be comparable to the interocular difference observed in the typical resampled data set.

From each resampled data set, weights ($\mathbf{w}$, $\mathbf{w}'$) and correlation coefficients (r) were recalculated as described above. One thousand such resamplings were performed. We recorded the number of times (N) that resampled values of r were less than the value obtained from the original data. This yielded an estimate of P as $N/1000$. Large P-values indicate that most resampling of the data would produce scalp topographies as different as the observed topographies. Conversely, small P-values indicate that the differences between the scalp topographies observed is highly unlikely to be due to chance alone. This analysis method uses the internal variability in the data to determine the reliability of a difference between two subsets.

The results of the statistical analysis are presented in Table 1. In 3 out of 12 hemifields the probability (P) that the observed differences were due to chance alone was very small (0.001 or less). In 3 additional hemifields this probability was 0.07 or less. In 5 of 6 subjects (all but MW) stimulation of at least one hemifield led to an interocular difference unlikely to be due to chance alone. As previously noted, data from MW had the lowest signal-to-noise ratio, with statistically-significant responses in less than half of the derivations.

In 4 subjects, asymmetries were observed in one hemifield but not in the other (JV, MC, RB and KP of Table 1). While the failure to observe

interocular differences in one subject (MW) may well be related to a low signal-to-noise, it is unlikely that this inter-hemifield difference can be explained on this basis, since signal and noise were comparable for either hemifield of stimulation (e.g. Fig. 2).

Dipole modeling

To determine whether the kind of interocular differences we observed were consistent with the notion of a duplicated representation of nasal fovea, we modeled the effects of this representation on the scalp topography of the VEPs. We modeled cortical generators of the VEPs by equivalent dipoles. For simplicity, we assumed that the dipoles lay in the plane of the electrodes. In the initial model (upper row of Fig. 4: Type I), a radial dipole was placed within the plane of the electrodes. It was positioned at a distance f from the center of the head equal to 0.7 of the head radius. The azimuth angle ϕ between the electrode position and the sagittal (midline) plane was equal to 20 deg ($\phi = 0$ deg denotes an occipital dipole positioned in the sagittal plane, and $\phi = 90$ deg denotes a dipole positioned in the coronal plane, pointing towards the right ear).

The locations chosen for the dipoles were determined from previous investigations of VEP topography. The value of f was the average of the value $f = 0.8$ determined by Butler *et al.* (1987) and $f = 0.6$ determined by Maier *et al.* (1987). The azimuth ϕ corresponding to the midpoint of the occipital representation of a 4 deg hemifield stimulus was taken to be 20 deg, from Darcey *et al.*'s (1980) measurement of the responses to a 5 deg field. The value $\phi = 20$ deg is also the approximate mean of the values $\phi = 30$ deg determined by Butler *et al.* (1987) for 1.6 deg fields and $\phi = 12$ deg determined by Maier *et al.* (1987) for 2 deg fields. These data are consistent with the direct but necessarily less-detailed intracranial study of Ducati *et al.* (1988).

In view of the wide variations in the anatomy of primary visual cortex among and within individuals (Stensaas *et al.*, 1974), we also considered models in which the cortical VEP generator was placed along the interhemispheric fissure (Fox *et al.*, 1986), rather than along the convexity. This is the Type III model of the first row of Fig. 4. The strength and position of the dipole was calculated by moving the dipole of the Type I model to the interhemispheric fissure. The Type II model was halfway between Type I and Type III, with half of the generating region moved into the interhemispheric fissure.

These three dipole geometries were used to model the response to 4 deg hemifield stimulation, assuming that only contralateral cortex was stimulated (top row of Fig. 4). For this modeling, the fields of dipoles within a standard three-sphere head model (scalp, skull and brain) were approximated by the fields of displaced equivalent dipoles within a uniform-sphere head model, according to the method of Ary *et al.* (1981). The dipole field, and responses as measured with our experimental montage, were calculated according to the formula of Fender (1987). The Type II geometry required calculation of the responses to two dipoles: one corresponding to the strip of cortex on the convexity, and one corresponding to the strip of cortex in the interhemispheric fissure. The resulting dipole fields were then superimposed.

To calculate responses predicted by a geometry which included bilateral activation by a parafoveal $\frac{1}{2}$ deg strip (bottom three rows of Fig. 4), we added an additional dipole. The position of this dipole within the cortex and its relative size were estimated from data of Dow *et al.* (1984), concerning the retino-cortical map in the macaque. From the data of Dow *et al.*, the extent of cortex subserving the central $\frac{1}{2}$ deg of vision is approx. 7.1 mm, while the extent of cortex subserving the central 4 deg of vision is approx. 19.8 mm. This ratio was used to place an equivalent dipole, according to geometries I, II and III, corresponding to a duplicated representation of the central $\frac{1}{2}$ deg. The foveal representation was placed most medially in the Type I model. To maximize the effect of differences in cortical geometry, the foveal representation was placed most anteriorly in the Type III model (corresponding to a single sliding of the generator into the interhemispheric fissure). In the Type II model, the foveal representation occupied an intermediate position, near the "bend" in the assumed geometry of the striate cortex. If the fovea is placed more posteriorly along the interhemispheric fissure, as would be appropriate according to the data of Fox *et al.* (1986), then the contribution of the duplicated foveal projection in the Type III model would appear similar to that in the Type II model considered here. We therefore do not consider this case separately. Predicted scalp topography for the various geometries of bilateral cortical

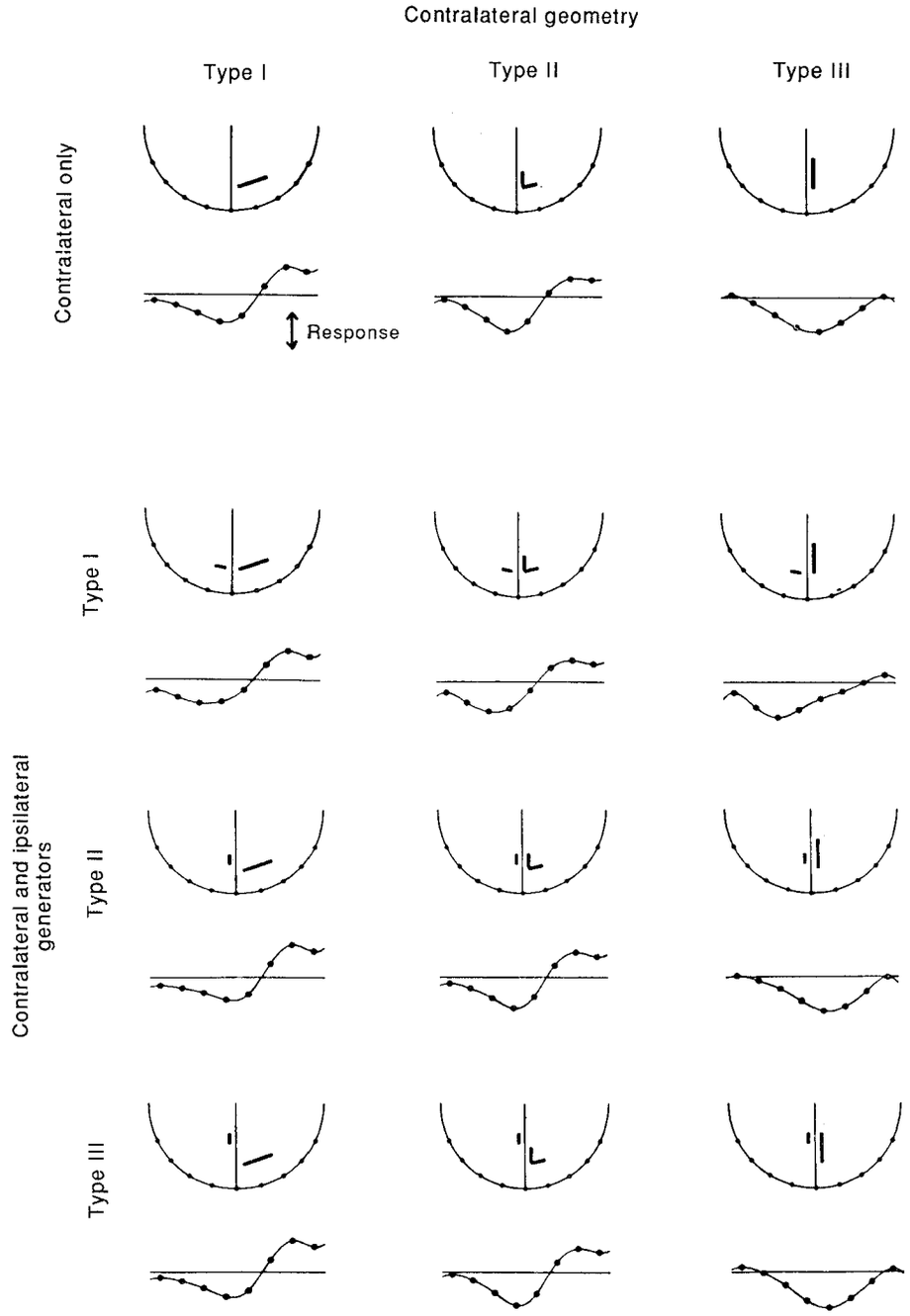

Fig. 4. Scalp distributions predicted from simple dipole models. The top row shows the spatial weights anticipated from contralateral-only projections from a single visual hemifield, with any of three alternate geometries for the primary visual cortex. The next three rows show the anticipated effect of adding an ipsilateral projection corresponding to bilateral representation of nasal foveal retina. In all diagrams, heavy bars represent the positions and sizes of cortical strips. Corresponding dipole generators are perpendicular to the illustrated bars, and point outward from the hemisphere.

activation was calculated by superimposing the scalp fields resulting from two dipoles (for Type I or Type III contralateral geometry) or three dipoles (for Type II contralateral geometry) in the three-sphere model (Ary *et al.*, 1981; Fender, 1987).

The last three rows of Fig. 4 show the predicted scalp topographies of spatial weights, for all three geometries in the hemisphere contralateral to the stimulus, and all three geometries in the hemisphere ipsilateral to the stimulus. Correlation coefficients r which express the differ-

ences between the contralateral-only geometry and the bilateral geometries are tabulated in Table 2.

Dipole modeling provided the following results. First, the differences in the spatial weights due to an additional generator are not large (compare curves in the last three rows of Fig. 4 with corresponding curves in the top row). Indeed, the predicted correlation coefficients range upward from 0.749 (Table 2) and are comparable to those derived from the actual data (Table 1). Second, in general, adding an ipsilateral dipole results in a slightly less unipolar weight function, i.e. the portion of the weight curve above and below the isopotential line becomes more nearly balanced. The clearest example of this is the comparison of the spatial weights for a contralateral Type II geometry in isolation (second entry on first row of Fig. 4), with the spatial weights when an ipsilateral Type I generator is added (second entry on second row of Fig. 4). The weight in the right paramedian lead moves towards zero when dipoles are present bilaterally. This is what was observed in the actual data sets which showed an obvious (though small) interocular difference. The movement towards zero occurs with stimulation of the eye *ipsilateral* to the hemifield (Fig. 3A–C). This implies that it is *nasal*, rather than temporal, retina which has a duplicated representation.

Third, Table 2 reveals that a Type I ipsilateral geometry produces the smallest correlation coefficient r (and the largest difference in topography), while Type II and Type III ipsilateral geometries lead to values of r which are only slightly less than 1 (and has very little effect on topography). This may explain why a larger interocular difference may be seen with stimulation of one hemifield than with the other (subjects JV, MC, RB and KP of Fig. 3 and Table 1). That is, the apparent unilateral nature of the asymmetry in VEP topography observed in some subjects may be explained by side-to-side variations in the position of primary visual cortex with respect to the convexity.

Table 2. Correlation coefficients (r) predicted from simple dipole models of Fig. 3

	Contralateral geometry		
Ipsilateral geometry	Type I	Type II	Type III
Type I	0.953	0.889	0.749
Type II	0.982	0.973	0.982
Type III	0.990	0.982	0.993

It is worth noting that none of the geometries considered provide a predicted scalp distribution which mimics the observed distribution in detail. This is not surprising considering the approximations and limitations of the modeling technique. A more realistic model would need to include multiple dipoles (Srebro, 1985; Sutter, 1988) whose orientations and positions are not constrained to lie in the plane of the electrode. Unfortunately, a general N-dipole model would have $6N$ free parameters. Even for $N = 1$, and especially for large N, this would be inappropriate to fit to a set of 8 measured weights. We therefore did not attempt to solve this underdetermined "inverse" problem but rather aimed to determine whether magnitude and direction of the effect observed are consistent with anatomical models.

DISCUSSION

We have demonstrated that there is an interocular difference in the topography of the VEP elicited by monocular hemifield stimulation. Though this difference is small, it was in excess of what might be expected by chance alone in all data sets with an acceptable signal-to-noise ratio. As shown by dipole modeling, this difference in the pattern of cortical activation is consistent with the hypothesis that the nasal fovea is bilaterally represented (Bunt *et al.*, 1977; Leventhal *et al.*, 1988). First we will examine possible alternative explanations for the interocular difference in VEP topography. Then, we will discuss its significance.

Exclusion of alternative explanations

Any asymmetry between the nasal and temporal retina might constitute a confounding factor in comparison of hemifield responses from the two eyes. One class of asymmetries is a difference in ganglion cell number (Perry and Cowey, 1985) or photoreceptor number (Curcio *et al.*, 1987). However, such asymmetries would merely change the overall size of the response. Since our analysis method normalizes for response size, these will not lead to the appearance of interocular differences in topography.

Another asymmetry is the greater peripheral extent of the temporal visual field (Harrington, 1981). This cannot explain our observed differences, because our stimuli were small (4 min) checks confined to the central 4 deg of vision,

which emphasizes the foveal contribution to the VEPs. Furthermore, because of the cortical magnification factor, the central 1 deg of vision is the main contributor to the scalp VEP (Sutter, 1985).

The observed interocular difference cannot be explained by the fact that we restricted the analysis only to the first principal component of the signal, or that higher even-order harmonics were discarded. Neglecting such additional components would result only in a *loss* of details concerning scalp topography, rather than a creation of artifactual differences.

It is well-known that practiced observers have residual miniature eye movements of the order of 10 min during fixation (Steinman *et al.*, 1973). However, it is unlikely that the observed differences in VEP topography result from such miniature eye movements. Imperfect fixation, if present in both eyes, would degrade, rather than create, any measured difference in scalp topography. Systematic interocular differences in fixation behavior is unlikely, given that our subjects had no visual field deficits, attention deficits, or oculomotor disturbances, and normal stereoscopic vision. Residual eye movements and nonfoveal fixation complicates precise mapping of monocular fields in patients with lesions affecting the visual system, but the confounding effects of these factors are minimized through the use of practiced normal observers.

We cannot exclude the possibility that the finding of an interocular difference in only one hemifield indicates that only one nasal fovea has a duplicated representation. However, as demonstrated by dipole modeling, this may simply be an effect of side-to-side variability in the geometry of the striate cortex. While we do not have anatomical confirmation of side-to-side variability of hemispheric geometry in our subjects, the asymmetries of the left hemifield and right hemifield responses within one eye (Fig. 3) support this notion. Side-to-side anatomical variability is commonplace (Stensaas *et al.*, 1974), and VEP evidence for such variability has previously been reported (Jeffreys and Axford, 1972).

Relationship to models of retino-calcarine projections

Mapping of retrograde transport of HRP from the primate LGN to the retina revealed a band of cells on the nasal side of the fovea which send their axons to the ipsilateral LGN (Leventhal *et al.*, 1988; Bunt *et al.*, 1977). If signals from these cells activate the striate cortex then the following can be predicted: stimulation of nasal retina will activate primary visual cortex contralateral to the stimulus as well as a portion of primary visual cortex ipsilateral to it. In contrast, stimulation of temporal retina would elicit only unilateral (i.e. ipsilateral) activation of primary visual cortex. Thus, the pattern of cortical activation by a given hemifield depends on the eye stimulated: viewing a hemifield with the ipsilateral eye produces bilateral activation while viewing of a hemifield with the contralateral eye produces only unilateral activation.

Our findings are consistent with this pattern of activation, and cannot readily be accounted for by alternative explanations. Monocular viewing of homonymous hemifields produces interocular differences in VEP topography. Furthermore, through dipole modeling techniques, we established that the size and nature of these differences agree with the pattern of bilateral cortical activation predicted by the retino-geniculate projections (Leventhal *et al.*, 1988). Thus, the bilateral representation of central nasal retina postulated in primates on anatomical basis is likely to be present also in man.

Two recent studies which addressed the issue of the representation of foveal vision were interpreted as showing no evidence for bilateral representation. Tootell *et al.* (1988) mapped retino-calcarine pathways by the 2-deoxyglucose method in primates, and found no evidence for bilateral representation of central vision. This finding contradicts a large body of evidence for bilateral representation of the vertical meridian (e.g. Hubel and Wiesel, 1967; Blakemore, 1969; Wong-Riley, 1974). The reason for the discrepancy is unclear. One possible explanation is that the relevant cortical neurons, which are presumably binocular and optimally activated by binocular stimuli, are not activated by monocular stimuli under anesthesia. Thus, their 2-deoxyglucose incorporation does not increase, and these neurons are not seen.

Fendrich and Gazzaniga (1989) examined visual matching across the vertical meridian in a patient whose corpus callosum was surgically sectioned. They concluded that the retinal projections were cleanly split on the basis of poor performance for targets straddling the meridian by as little as 30 min. However, although per-

formance was markedly degraded when stimuli straddled the meridian, it was still above chance at four of five target locations within 1 deg of the meridian. Although these authors emphasize the *relative* lack of an ipsilateral nasal projection, their findings suggest that this projection does indeed exist.

One possibility that we cannot entirely exclude is that the interocular difference in scalp topography is due to callosal connections, rather than bilateral projection at the subcortical level. Callosal connections could only account for an interocular difference in scalp topography if callosal fibers originate preferentially in cortical units which receive input from the nasal hemiretina of the contralateral eye. One study in the cat (Voigt *et al.*, 1988) suggests that striate cells which project via the corpus callosum are grouped in a patchy fashion. If these patches indeed correspond to ocular dominance columns, then callosal connections may play a role in our findings. However, studies in the primate (Kennedy *et al.*, 1986; Gould *et al.*, 1987) do not suggest a columnar organization of striate neurons that project via the corpus callosum.

Relevance to macular sparing and splitting

The terms macular sparing and macular splitting refer to the degree of involvement of the central vision after brain lesions affecting the visual pathways (Bunge, 1884; Putnam and Liebman, 1942; Williams and Gassel, 1962). In "macular sparing", central vision is preserved in an otherwise hemianopic field. In "macular splitting", the blind region extends to the vertical meridian, through the macula as well as more peripherally. The physiologic basis of these phenomena is a matter of longstanding controversy.

In the vast majority of well-documented cases of macular sparing, the region of sparing does not extend to the entire portion of visual space viewed by the macula (about 6 deg). Since the typical region of sparing better matches the visual space viewed by the fovea (1–2 deg), the terms "foveal" sparing and splitting are more appropriate (Huber, 1962).

Foveal sparing is more frequent in patients with lesions of the occipital lobe and posterior optic radiations, while foveal splitting is more common in patients with lesions of the anterior post-chiasmatic visual pathways (Putnam and Liebman, 1942). This classic clinical teaching is based on many studies of patients whose pathways were lesioned by a wide variety of pathological processes (Horrax and Putnam, 1932; Penfield *et al.*, 1935; Huber, 1962; Williams and Gassel, 1962; Koerner and Teubner, 1973).

Leventhal *et al.* (1988) have proposed that the bilateral representation of the nasal fovea is the neural substrate of macular sparing and splitting. Our study indicates that a bilateral projection of nasal retina is likely to exist in man and that it produces cortical activation. Though this projection pattern may contribute to foveal sparing, it is unlikely to account for its full clinical spectrum. If the bilateral foveal projection were the sole cause of foveal sparing, then lesions in the anterior post-chiasmatic optic pathways would be as likely as posterior lesions to produce the phenomenon. But, foveal sparing is more frequent in occipital lobe lesions than in optic tract lesions (Putnam and Liebman, 1942). Another problem with the notion that a duplicated nasal retinal projection accounts for foveal sparing is that it predicts a unilateral sparing of the fovea in complete lesions of the optic tract. This is not consistent with the clinical observations of Newman and Miller (1983) who reported normal visual acuity in both eyes of their patients. On the other hand, eight of the twelve patients reported by Bender and Bodis-Wollner (1978) had marked reductions in acuity or central scotoma only on the involved side, consistent with the present prediction. While a duplicated foveal projection may contribute to sparing and splitting, alternative explanations, including a separate blood supply to the foveal representation, the large cortical magnification factor for the foveal representation, and altered fixation behavior in hemianopic patients, may also pay a role (Miller, 1982, pp. 145–147).

Relevance to binocular vision near the vertical meridian

The absence of a perceptual discontinuity in the visual fields at the vertical meridian suggests that there must be some neutral mechanism for encoding visual information pertaining to the meridian region in both hemispheres. While a variety of mechanisms for bilateral representation of the midline retina have been proposed (Putnam and Liebman, 1942), only two seem likely in view of current anatomical and physiological data. One is that there are connections between visual cortices which travel through the posterior aspect of the corpus callosum. This

has been confirmed electrophysiologically (Hubel and Wiesel, 1967) and by axonal transport studies (Wong-Riley, 1974). The other mechanism is bilateral projection of the midline retina, as recently demonstrated by HRP studies (Bunt *et al.*, 1977; Leventhal *et al.*, 1988). Since the duplication of the foveal projection is only partial, these two mechanisms must both be involved in order to assure continuity of the visual field at the midline.

As Blakemore (1969) lucidly pointed out, in order to assure that binocular vision is present in areas of space in front of and behind the fixation point, the retinal midline needs to be bilaterally represented. Furthermore, to allow for one hemisphere to view all of the contralateral hemifield when the eyes are converged, there must be a duplication of the foveal projections (Fig. 1, upper panel). Our data suggest that this strip of duplication exists. However, in contrast to Blakemore's view (1969), we find evidence that this duplicate projection involves primarily (or exclusively) the nasal fovea. Duplication of the nasal fovea provides the substrate for binocular vision only beyond the fixation point, and not in front of fixation. In this regard, it is interesting to note that the extent of nasal retina which has a bilateral representation is similar to Panum's fusional area, approx. 1 deg (Fender and Julesz, 1967). Duplication of the projection from nasal side of the fovea is in some sense more efficient than duplication of the projection from the temporal side: the duplicated nasal projection will provide binocular input over a greater volume of the relevant visual space when the eyes are converged.

If the duplicated nasal projection is relevant to stereopsis near the vertical meridian, one might expect selective enhancement in processing of uncrossed disparity at the fovea, relative to processing of uncrossed disparity in more eccentric locations along the vertical meridian. Manning *et al.* (1987) found this result, as well as impaired processing of uncrossed disparity at 3 deg above or below fixation as compared with 3 deg left to right of fixation. At all retinal locations studied, thresholds for crossed disparity were substantially shorter than those for uncrossed disparity, and thresholds for crossed disparity were similar for central stimuli and for stimuli at 3 deg eccentricity in any direction. Thus, the dependence of crossed and uncrossed detection thresholds on retinal location appears to be a result of at least two factors: a large superiority for the processing of crossed disparity at all locations, and a selective enhancement for processing of uncrossed disparity at the center of gaze. The physiologic basis for the former has been hypothesized to be distinct pools of neurons for crossed and uncrossed disparity (Manning *et al.*, 1987; Fischer and Poggio, 1979); we postulate that duplication of the representation of nasal fovea is related to the latter.

In conclusion, we have demonstrated an interocular difference in the pattern of cortical activation produced by monocular hemifield stimulation. The pattern of cortical activation suggests that in man, as well as in primates, there is bilateral projection of the nasal fovea. While the finding helps to understand the continuity of the visual fields at the meridian and of stereopsis, it does not contribute to clarify the clinical problem of macular sparing and macular splitting.

Acknowledgements—We wish to thank Dr F. Plum for directing our attention to the paper of Leventhal *et al.* (1988) and Dr Keith Purpura for providing many helpful comments on a draft of this manuscript. Portions of this work have been presented in abstract form (Iadecola *et al.*, 1989). This work was supported in part by grants EY7977 and NS877.

REFERENCES

Ahlberg J. H., Nilson E. N. and Walsh J. L. (1967) *The Theory of Splines and Their Applications*. Academic Press, New York.

Ary J. P., Klein S. A. and Fender D. H. (1981) Location of sources of evoked scalp potentials: correction for skull and scalp thickness. *IEEE Trans. Biomed. Engng* **BME-28,** 447–452.

Barrett G., Blumhard L., Halliday A. M., Halliday E. and Kriss A. (1976) Paradoxical reversal of lateralization of the half-field pattern-evoked response with monopolar and bipolar electrode montages. *J. Physiol., Lond.* **258,** 63–64P.

Bender M. B. and Bodis-Wollner I. (1978) Visual dysfunction in optic tract lesions. *Ann. Neurol.* **3,** 187–193.

Blakemore C. (1969) Binocular depth discrimination and the nasotemporal division. *J. Physiol., Lond.* **205,** 471–497.

Bunge P. (1884) Ueber gesichtsfeld und faservelauf in optischen lietungsapparat, Habilitationsschrift, M. Niemeyer, Halle.

Bunt A. H., Minckler D. S. and Johanson G. W. (1977) Demonstration of bilateral projection of the central retina of the monkey with horseradish peroxidase neuronography. *J. comp. Neurol.* **171,** 619–630.

Butler S. R., Georgiu G. A., Glass A., Hancox R. J., Hopper J. M. and Smith K. R. H. (1987) Cortical generators of the CI component of the pattern-onset visual evoked potential. *Electroenceph. clin. Neurophysiol.* **68,** 256–267.

Cobb W. A. and Morton H. B. (1970) Evoked potentials from the human scalp to visual half-field stimulation. *J. Physiol., Lond.* **208,** 39–40P.

Curcio C. A., Sloan K. R. Jr, Packer O., Hendrickson A. E. and Kalina R. E. (1987) Distribution of cones in human and monkey retina: individual variability and radial asymmetry. *Science* **236,** 579–582.

Darcey T. M., Ary J. P. and Fender D. H. (1980) Methods for the localization of electrical sources in the human brain. In *Motivation, Motor and Sensory Processes of the Brain, Progress in Brain Research*, edited by Kornhuber H. H. and Deecke L., Vol. 54, pp. 128–134. Elsevier, Amsterdam.

Dow B. M., Vautin R. G. and Bauer R. (1984) The mapping of visual space onto foveal striate cortex in the macaque monkey. *J. Neurosci.* **5,** 890–902.

Ducati A., Fava E. and Motti E. D. F. (1988) Neuronal generators of the visual evoked potentials: intracerebral recording in awake humans. *Electroenceph. clin. Neurophysiol.* **71,** 89–99.

Efron B. (1980) The jacknife, the bootstrap and other resampling plans. Technical Report No. 63, Division of Biostatistics, Stanford University, Stanford, CA.

Fender D. H. (1987) Source localization of brain activity. In *Handbook of Electroencephalography and Clinical Neurophysiology*, edited by Gevins A. S. and Remond A., Vol. 1, Revised Series, pp. 355–405. Elsevier, Amsterdam.

Fender D. H. and Julesz B. (1967) Extension of Panum's fusional area in binocularly stabilized vision. *J. opt. Soc. Am.* **57,** 819–830.

Fendrich R. and Gazzaniga M. S. (1989) Evidence of foveal splitting in a commissurotomy patient. *Neuropsychologia* **27,** 273–281.

Fischer R. and Poggio G. F. (1979) Depth sensitivity of binocular cortical neurons of behaving monkeys. *Proc. R. Soc. Lond. B* **204,** 409–414.

Fox P. T., Mintun M. A., Raichle M. E., Miezin F. M., Allman J. M. and Van Essen D. C. (1986) Mapping human visual cortex with positron emission tomography. *Nature, Lond.* **323,** 806–809.

Gould H. J. III, Weber J. T. and Rieck R. W. (1987) Interhemispheric connections in the visual cortex of the squirrel monkey (*Saimiri sciureus*). *J. comp. Neurol.* **256,** 14–28.

Gutowitz H., Zemon V., Victor J. D. and Knight B. W. (1986) Source geometry and dynamics of the visual evoked potential. *Electroenceph. clin. Neurophysiol.* **64,** 308–327.

Halliday A. M. and Michael W. F. (1970) Changes in pattern-evoked responses in man associated with the vertical and horizontal meridians of the visual field. *J. Physiol., Lond.* **208,** 499–513.

Harrington D. O. (1981) *The Visual Fields*, 5th edn. Mosby, St Louis, MO.

Horrax G. and Putnam T. J. (1932) Distortion of the visual fields in cases of brain tumor. *Brain* **55,** 499–523.

Hubel D. H. and Wiesel T. N. (1967) Cortical and callosal connections concerned with the vertical meridian of visual fields in the cat. *J. Neurophysiol.* **30,** 1561–1573.

Huber A. (1962) Homonymous hemianopia after occipital lobectomy. *Am. J. Ophthal.* **54,** 623–629.

Iadecola C., Conte M. M. and Victor J. D. (1989) Does bilateral cortical representation of temporal visual fields exist in man? *Soc. Neurosci. Abstr.* **15,** 118.

Jeffreys D. A. and Axford J. G. (1972) Source locations of pattern-specific components of human visual evoked potentials—I. Component of striate cortical origin. *Expl Brain Res.* **16,** 1–21.

Kennedy H., Dehay C. and Bullier J. (1986) Organization of the callosal connections of visual areas V1 and V2 in the macaque monkey. *J. comp. Neurol.* **247,** 398–415.

Koerner F. and Teubner H. L. (1973) Visual field defects after missile injuries of the geniculo-striate pathways in man. *Expl Brain Res.* **18,** 88–113.

Leventhal A. G., Ault S. J. and Vitek D. J. (1988) The nasotemporal division of the primate retina: the neural bases of macular sparing and splitting. *Science* **240,** 66–67.

Maier J., Dagnelie G., Spekreijse H. and Van Dijk B. W. (1987) Principal component analysis for source localization of VEPs in man. *Vision Res.* **27,** 165–177.

Manning M. L., Finlay D. C., Neill R. A. and Frost B. G. (1987) Detection threshold differences to crossed and uncrossed disparities. *Vision Res.* **27,** 1683–1686.

Milkman N., Schick G., Rossetto M., Ratliff F., Shapley R. and Victor J. D. (1980) A two-dimensional computer-controlled visual stimulator. *Behav. Res. Meth. Instrum.* **12,** 283–292.

Miller N. R. (1982) *Walsh and Hoyt's Clinical Neuro-Ophthalmology*, 4th edn, Vol. 1. Williams & Wilkins, Baltimore, MD.

Morax V. (1919) Discussion des hypotheses faites sur le connexions corticales des faiescieaux maculaires. *Ann. Oculist., Paris* **156,** 1–25.

Newman S. A. and Miller N. R. (1983) Optic tract syndrome. Neuro-ophthalmologic considerations. *Archs Ophthal.* **101,** 1241–1250.

Penfield W., Evans J. P. and MacMillan J. A. (1935) Visual pathways in man with particular reference to macular representation. *Archs neurol. Psychiat., Chicago* **13,** 816–834.

Perry V. H. and Cowey A. (1985) The ganglion cell and cone distributions in the monkey's retina: implications for central magnification factors. *Vision Res.* **25,** 1795–1810.

Polyak S. (1934) Projection of the retina upon the cerebral cortex based upon experiments with monkey. *Annals of Nervous and Mental Disorders*, pp. 535–557. Williams & Wilkins, Baltimore, MD.

Putnam T. J. and Liebman S. (1942) Cortical representation of the macula lutea. *Archs Ophthal.* **28,** 415–443.

Srebro R. (1985) Localization of visually evoked cortical activity in humans. *J. Physiol., Lond.* **360,** 233–246.

Steinman R. M., Haddad G. M., Skavenski A. A. and Wyman D. (1973) Miniature eye movement. *Science* **181,** 810–819.

Stensaas S. S., Eddington D. E. and Dobelle W. H. (1974) The topography and variability of the primary visual cortex in man. *J. Neurosurg.* **40,** 747–755.

Stone J., Leicester J. and Sherman S. M. (1973) The naso-temporal division of the monkey's retina. *J. comp. Neurol.* **150,** 333–348.

Sutter E. (1985) Multi-input VER and ERG analysis for objective perimetry. *IEEE Seventh Annual Conf. Engineering in Medicine and Biology Society*, Chicago, pp. 414–420.

Sutter E. (1988) Field topography of the visual evoked response. *Invest. Ophthal. visual Sci.* **29** (Suppl.), 433.

Tootell R. B. H., Switkes E., Silverman M. S. and Hamilton S. L. (1988) Functional anatomy of the macaque striate cortex—II: retinotopic organization. *J. Neurosci.* **8,** 1531–1568.

Victor J. D. and Mast J. (1991) A new statistic for steady-state evoked potentials. *Electroenceph. clin. Neurophysiol.* **78,** 378–388.

Voigt T., LeVay S. and Stamnes M. A. (1988) Morphological and immunocytochemical observations on the visual callosal projections in the cat. *J. comp. Neurol.* **272,** 450–460.

Williams D. and Gassel M. M. (1962) Visual function in patients with homonymous hemianopia—Part I. The visual fields. *Brain* **85,** 175–250.

Wong-Riley M. T. T. (1974) Demonstration of geniculocortical and callosal projection neurons in the squirrel monkey by means of retrograde axonal transport of horseradish peroxidase. *Brain Res.* **79,** 267.